OXFORD

JNCI J Natl Cancer Inst (2018) 110(9): djy003

doi: 10.1093/jnci/djy003
First published online February 22, 2018
Article

ARTICLE

Novel Dual-Action Targeted Nanomedicine in Mice With Metastatic Thyroid Cancer and Pancreatic Neuroendocrine Tumors

Naris Nilubol*, ZiQiang Yuan*, Giulio F. Paciotti, Lawrence Tamarkin, Carmen Sanchez, Kelli Gaskins, Esther M. Freedman, Shugeng Cao, Jielu Zhao, David G. I. Kingston, Steven K. Libutti†, Electron Kebebew†

See the Notes section for the full list of authors' affiliations.
Correspondence to: Naris Nilubol, MD, Endocrine Oncology Branch, National Cancer Institute, Clinical Research Center, 10 Center Drive, Rm. 45932, Bethesda, MD 20892 (e-mail: niluboln@mail.nih.gov).
*Authors contributed equally to this work and are co-first authors.
†Authors contributed equally to this work and are co-senior authors.

Abstract

Background: The advantages of nanomedicines include preferential delivery of the payload directly to tumor tissues. CYT-21625 is the novel, first-in-class gold nanomedicine designed to target tumor vasculature and cancer cells by specifically delivering recombinant human tumor necrosis factor alpha (rhTNF) and a paclitaxel prodrug.
Methods: We analyzed TNF receptor expression in publicly available gene expression profiling data and in thyroid tissue samples. Mice with metastatic FTC-133 and 8505C xenografts and the *MEN1* conditional knock-out mice were treated weekly with CYT-21625 and gold nanoparticles with rhTNF only (CYT-6091); controls included mice treated with either paclitaxel or saline. In vivo luciferase activity was used to assess the effects on tumor growth. Computed tomography, magnetic resonance imaging, and 18F-Fludeoxyglucose positron emission tomography were used to study tumor selectivity in mice with insulin-secreting pancreatic neuroendocrine tumors (PNETs). All statistical tests were two-sided.
Results: Anaplastic thyroid cancer (ATC) expressed statistically significantly higher levels of TNF receptor superfamily 1A and 1B messenger RNA ($n = 11$) and protein ($n = 6$) than control samples ($n = 45$ and 13, respectively). Mice ($n = 5$–7 per group) with metastatic ATC ($P < .009$) and FTC-133 xenografts ($P = .03$ at week 3, but not statistically significant in week 4 owing to reduced sample size from death in non-CYT-21625 groups) treated with CYT-21625 had a statistically significantly lower tumor burden. Treatment with CYT-21625 resulted in loss of CD34 expression in intratumoral vasculature, decreased proliferating cell nuclear antigen, and increased cleaved caspase-3. Intratumoral vascular leakage occurred only in mice with PNET and ATC treated with CYT-6091 and CYT-21625. CYT-6091 and CYT-21625 preferentially deposited in PNETs and statistically significantly decreased serum insulin levels ($n = 3$ per group, $P < .001$). There were no toxicities observed in mice treated with CYT-21625.
Conclusions: CYT-21625 is effective in mice with PNETs and metastatic human thyroid cancer with no toxicities. Thus, CYT-21625 should be studied in patients with advanced PNETs and thyroid cancer.

The current treatment options for patients with dedifferentiated thyroid cancer refractory to radioactive iodine treatment include multikinase inhibitors such as sorafenib and lenvatinib (1,2). However, serious adverse events requiring either a dose reduction or a treatment interruption because of toxicities occur in 37% of patients treated with sorafenib and in 75% of patients

Received: August 2, 2017; **Revised:** October 12, 2017; **Accepted:** January 8, 2018

treated with lenvatinib (1,2). Lastly, no durable complete responses have been observed with sorafenib and lenvatinib therapy in radioiodine-negative, differentiated, or poorly differentiated thyroid cancer.

Anaplastic thyroid cancer (ATC) is a rare and lethal subtype of thyroid cancer, accounting for less than 2% of all thyroid cancers but approximately one-third of thyroid cancer–specific deaths (3). The median survival rate of patients with ATC is less than six months, with 90% of patients presenting with unresectable and metastatic disease at the time of diagnosis (4,5). Currently, there is no effective therapy for ATC, and patient survival has not improved in more than six decades (5,6). Thus, it is critically important to identify new treatment that inhibits disease progression or metastasis and improves the survival rate of patients with ATC.

The annual incidence of pancreatic neuroendocrine tumors (PNETs) is continuously increasing within the United States and is estimated to be three to five cases per 100 000 inhabitants (7–9). Nonfunctioning PNETs account for more than 85% of all neuroendocrine tumors of the pancreas and present with distant metastases in up to 60% of cases (10–12). The current approved systemic therapy for patients with advanced PNETs includes somatostatin analogs and targeted therapy such as sunitinib and everolimus. However, a durable partial is uncommon with these treatments. Sunitinib and everolimus have clinically significant toxicity, and dose reduction or treatment interruption is commonly required (13,14).

A major limitation to systemically delivered cancer therapies is dose-limiting toxicity due to off-target activity resulting in injury to normal cells and tissues. Because solid tumors have highly permeable vasculature and high cell density but low lymphatic drainage, the tumor interstitial fluid pressure (IFP) is higher than surrounding normal tissue. The elevated IFP results in a drop of convection between the intra- and extravascular spaces, thus limiting drug distribution into the tumor microenvironment and markedly reducing its efficacy (15). Current anticancer drugs do not address this limitation. Hypervascularity is common in endocrine cancers such as thyroid cancer and PNETs (16,17). Thus, these two cancers are suitable models to demonstrate the efficacy of nanomedicine that disrupts tumor blood vessels to enhance the delivery of cytotoxic agents. Nanomedicines offer the promise of overcoming this limitation by allowing for the design of agents that can selectively deliver their payload to tumor tissues (18). The novel, first-in-class nanomedicine CYT-21625 comprises two distinct antitumor agents, recombinant human tumor necrosis factor alpha (rhTNF) and a paclitaxel prodrug analog (JZ-21625), bound to gold particles. CYT-21625 selectively targets solid tumors passively by the enhanced permeability and retention (EPR) effect and actively by rhTNF binding to its receptors on the tumor neovasculature and induces apoptosis of vascular endothelium, destroying tumor blood vessels. CYT-21625 in the tumor releases native paclitaxel that exerts a direct antitumor effect. Because the release of the paclitaxel analog on CYT-21625 requires elevated levels of glutathione (GSH) in the tumor microenvironment (19), such a condition cannot be recapitulated in vitro. Thus, the aims of this study were to determine the in vivo antitumor activity of CYT-21625 in transgenic and metastatic models of endocrine cancers and to evaluate the mechanism of action of CYT-21625 treatment in these models.

ARTICLE

Methods

CYT-6091 and CYT-21625

CYT-6091 and the colloidal gold nanoparticles used for CYT-21625 production were prepared per a previously published protocol (20). We described the production of CYT-21625 and dosages in the Supplementary Materials (available online).

Cell Lines

The 8505C and FTC-133 thyroid cancer cell lines do not express thyroglobulin, thyroid-stimulating hormone receptor, thyroid peroxidase, or sodium-iodine symporter genes consistent with dedifferentiated thyroid cancer (21). These cell lines were authenticated by short tandem repeat. Both the 8505C and FTC-133 cells were transfected with a linearized pGL4.51[*luc2*/CMV/Neo] vector (Promega, Madison, WI) encoding the luciferase reporter gene *luc2* (*Photinus pyralis*) as previously described (22). The sources, characteristics, and culture conditions of these cell lines are described in the Supplementary Materials (available online).

Gene Expression Profiling of Anaplastic Thyroid Cancer

We analyzed publicly available, genome-wide expression data (GSE33630, Gene Expression Omibus, The National Cancer for Biotechnology Information [23]) to study the messenger RNA expression of TNF receptors (*TNFRSF1A* and *TNFRSF1B*) in ATC samples compared with normal thyroid tissue. The Affymetrix U133 Plus 2.0 array was used to profile the gene expression of 11 ATCs, 49 papillary thyroid carcinomas (PTCs), and 45 normal thyroid samples (24).

Study Approval

The Animal Care and Use Committee (National Cancer Institute/National Institutes of Health) approved the thyroid cancer cell xenograft animal study protocol. All animal experiments involving MEN-1 conditional knock-out mice were conducted with approval from the Animal Ethical and Welfare Committee of Albert Einstein College of Medicine, based on procedures outlined in the National Institutes of Health Guideline for the Care and Use of Animals.

In Vivo Metastatic Poorly Differentiated and Anaplastic Thyroid Cancer Mouse Models

Luc2 reporter cells from a 70%–80% confluent monolayer culture were trypsinized and suspended in DMEM. Suspensions of 1×10^5 8505C-*Luc2* cells and 4×10^5 FTC-133-*Luc2* cells in 0.2 mL of DMEM were injected intravenously via tail vein into eight-week-old to three-month-old NOD.*Cg-Prkdc*^{scid} *Il2rg*^{tm1Wjl}/SzJ mice. We previously described the cell numbers required for each cell line to engraft with optimal survival (22). Mice were maintained under normal immunodeficient mouse care conditions and monitored daily to assess their health status. Mice were randomly assigned into treatment and control groups (n = 23 in the 8505C group, n = 7 in the vehicle control group, n = 6 in the CYT-6091 group, n = 5 in the paclitaxel and CYT-21625 groups, and n = 20 in the FTC-133 group; n = 5 per group). Treatment with CYT-21625 and controls started one week after implantation. We performed a bioluminescence imaging study weekly. To assess

vascular leakage, six mice with 8505C xenografts received one dose of CYT-21625 (n = 2), CYT-6091 (n = 2), paclitaxel (n = 1), and vehicle control (n = 1), then were euthanized 24 hours after treatments. The imaging, anesthetic, and euthanization techniques are described in the Supplementary Materials (available online).

The *MEN1* Conditional Knock-out Model With Pancreatic Neuroendocrine Tumors

Because insulinoma is the most common functioning PNET and the most common somatic mutation in PNETs is *MEN1* mutations (25), we selected a previously published *MEN1* conditional knock-out mouse model. These mice developed insulinomas with markedly elevated serum insulin and abnormal vasculature with increased vascular endothelial growth factor expression (26). Twelve 12-month-old mice carrying the *MEN1* allele flanked by loxP sites with Cre recombinase under the control of the pancreas-specific transcription factor *Pdx1* promoter (*Pdx1-Cre:Men1 floxed/floxed*) were used in this study. The mice were assigned to four groups treated with either CYT-6091 (n = 3), CYT-21625 (n = 3), paclitaxel (n = 3), or vehicle control (n = 3), respectively. The duration of the treatments was two weeks. The therapeutic responses to CYT-21625, CYT-6091, and paclitaxel were evaluated by measuring serum insulin levels. The in vivo biodistribution and vascular effects were monitored by computed tomography/positron emission tomography (CT/PET) and magnetic resonance imaging (MRI), respectively, as described in the Supplementary Materials (available online).

Enzyme-Linked Immunosorbent Assay for Insulin Level Measurement

The mice underwent a 24-hour fast prior to collection of whole blood via a retro-orbital bleeding technique, weekly. Serum insulin was measured by enzyme-linked immunosorbent assay (ELISA) with the Ultrasensitive Mouse Insulin ELISA kit (Mercodia, Inc.; Uppsala, Sweden) according to the manufacturer's instructions.

Immunohistochemistry and Immunofluorescence

Formalin-fixed tissues were embedded in paraffin and cut into 5 μm–thick sections for hematoxylin and eosin staining and immunostaining. To assess the protein expression of TNFRSF1A in human samples, we used a thyroid tissue microarray containing six cases of each normal thyroid tissue, follicular adenoma, PTC, FTC, and ATC (TH641, US Biomax, Inc., Rockville, MD). Three additional PTC samples (one with adjacent normal thyroid tissue) were used. Each case had duplicate samples. To assess TNFRSF1A expression in PNETs, we used 12 PNET samples from six patients with MEN1 syndrome (World Health Organization [WHO] grade 1 in 3 samples and grade 2 in 3 samples) and six patients with von Hippel-Lindau disease (WHO grade 1 in 2 samples and grade 2 in 4 samples). The methods used in immunohistochemistry and immunofluorescence are described in the Supplementary Materials (available online).

Statistical Analysis

We analyzed the gene expression profiling data (GSE33630) using embedded interactive statistical software (GEO2R). The *P* values were adjusted for false discovery rate using the Benjamini and Hochberg method (27). The fold change between groups was presented in a log2 scale. The Student *t* test was used to assess the difference in luciferase activity in mice treated with CYT-21625 and control groups (28). Overall survival (OS) was calculated in days from the implantation to the date of death. The Kaplan-Meier estimator (29) with log-rank (Mantel-Cox) (30) test was used to compare OS between groups. We used analysis of variance (ANOVA) with post hoc tests to compare the immunohistochemistry scores and the weight of mice between groups. We used luciferase activity and OS as the primary outcome measures in this study. Statistical analyses were performed using SPSS version 21.0 for Windows (SPSS, Inc., Chicago, IL). GraphPad Prism 6, version 6.01 (GraphPad Software, La Jolla, CA), was used to create graphs demonstrating in vivo luciferase activity.

The data from dynamic contrast-enhanced magnetic resonance imaging (MRI-DCE) were extracted using the Medical Image Processing, Analysis, and Visualization (MIPAV) program (National Institutes of Health, Bethesda, MD) created on Perl 5 (version 5). We used R (version 3.2.2) (31) to remove the outliers due to noise and motion, to draw the best-fit line, and to calculate area under the curve (AUC). The Kaplan-Meier estimator (29) with log-rank (Mantel-Cox) (30) test was used to compare OS between groups. Insulin serum is represented as the mean ± standard deviation. The difference between means was analyzed with either the two-tailed independent Student *t* test for two-group analysis, or by one-way ANOVA for analyses of three or more groups. If interactions were found, pair-wise comparisons between group levels were calculated with Bonferroni correction for multiple testing. A two-tailed *P* value of less than .05 was considered statistically significant.

Results

Expressions of Tumor Necrosis Factor Receptors in Differentiated Thyroid Cancer, Anaplastic Thyroid Cancer, and Pancreatic Neuroendocrine Tumors

Because the action of rhTNF is mediated through binding its receptors, we first evaluated TNF receptor expression in human cancer samples. The tumor necrosis factor receptor superfamily 1A (*TNFRSF1A*) and 1B (*TNFRSF1B*) mRNA expressions in ATC (n = 11) were statistically significantly higher than in normal thyroid tissue (n = 45) with an adjusted *P* value of less than .001 and fold change of 1.44 for *TNFRSF1A*, and an adjusted *P* value of less than .001 and fold change of 2.46 for *TNFRSF1B* (Figure 1A). Immunohistochemistry showed no TNFRSF1A expression in normal and benign thyroid tissue, except for one sample of follicular adenoma that had mild to moderate TNFRSF1A expression in intratumoral blood vessels (n = 13). Eight of 15 differentiated thyroid cancer (PTC and FTC) samples were positive for TNFRSF1A expression in intratumoral blood vessels (Figure 1, B and C). All six ATC samples had positive TNFRSF1A protein expression in intratumoral blood vessels and/or tumor cell cytoplasms (Figure 1D). ATC had a statistically significantly higher immunohistochemistry score of TNFRSF1A expression compared with differentiated thyroid cancer samples (papillary thyroid cancer [PTC] and follicular thyroid cancer [FTC], $P < .001$) and normal and benign thyroid samples ($P < .001$) (Figure 1E). Metastatic human ATC (8505C) and PDTC (FTC-133) lung xenografts expressed TNFRSF1A while myocardium adjacent to the tumors did not (Figure 1F). Of 12 primary PNET

samples, eight expressed TNFRSF1A in intratumoral blood vessels, including one sample with cytoplasmic TNFRSF1A expression. Adjacent normal pancreas and islet cells (n = 1) did not express TNFRSF1A (Figure 1G).

The Effects of CYT-21625 in Mice With Metastatic Human Anaplastic Thyroid Cancer and Follicular Thyroid Cancer Xenografts

Mice with metastatic human ATC xenografts (8505C cell line) treated with CYT-21625 for three weeks (once-a-week dosing) had statistically significantly less tumor burden, as demonstrated by a statistically significantly lower level of luciferase activity (vehicle vs CYT-21625: $P = .03$ week 2 and $P = .009$ week 3, and CYT-6091 vs CYT-21625: $P = .007$ week 2 and $P = .01$ week 3). There was no difference in luciferase activity between the vehicle control group and the CYT-6091-treated group ($P = .47$ week 2 and $P = .31$ week 3) (Figure 2A). All mice were euthanized after three weeks of treatments at the same time for humane end points because mice in vehicle control and CYT-6091 were in distress.

Next, we studied the effect of CYT-21625 in mice with metastatic human FTC xenografts (FTC-133). Although the luciferase activity in the CYT-21625 group was statistically significantly lower than that of other groups after three weeks of treatments ($P = .03$) and lower than the baseline activity in all mice treated with CYT-21625 for four weeks, the difference between groups after four weeks of treatments did not reach statistical significance (vehicle vs CYT-21625: $P = .06$, paclitaxel vs CYT-21625: $P = .35$, CYT-6091 vs CYT-21625: $P = .33$) because of reduced sample size, as three mice in the non-CYT-21625 group died after week 3 treatment (Figure 2B). Mice treated with CYT-21625 had statistically significantly longer overall survival (OS) than mice in the vehicle control and paclitaxel groups (mean OS = 52.2 days, 95% confidence interval [CI] = 49.0 to 55.3 days, vs mean OS = 41.7 days, 95% CI = 37.4 to 46.0 days, $P = .01$). There was no statistically significant difference in OS between mice in the CYT-21625 group and those in CYT-6091 group (mean OS = 52.2 days, 95% CI = 49 to 55.3 days, vs mean OS = 46.8 days, 95% CI = 39 to 54.6 days, $P = .32$) (Figure 2B).

There was no difference in weight between treatment groups (week 3 $P = .67$, week 4 $P = .33$). We observed asymptomatic mucosal and skin hyperpigmentation due to gold particle deposition in all mice treated with CYT-21625 (data not shown).

The Effects of CYT-21625 on Vascular Endothelium, Vascular Permeability, and Thyroid Cancer Cells in Metastatic Human Thyroid Cancer Xenografts

Human ATC xenografts weakly expressed TNFRSF1A in the cytoplasm but not in mouse vascular endothelium. Because CYT-21625 is thought to selectively target solid tumor neovasculature passively by the EPR effect and actively by rhTNF, we evaluated the disruption of intratumoral vascular endothelium in human ATC xenografts from the lungs by CD34 immunohistochemistry. Compared with the vehicle control, paclitaxel, and CYT-6091 groups, intratumoral vascular endothelium of human ATC xenografts in mice treated with CYT-21625 had no CD34 expression, consistent with endothelial damage (Figure 3A). However, there was no histologic evidence of normal organ (heart, liver, and kidneys) injuries or vascular endothelial damage in mice treated with CYT-21625 as demonstrated by retained CD34 endothelial cell expression (Figure 3, B and C). There was some deposit of gold nanoparticles, predominantly in the liver, without evidence of inflammation or any other morphologic and histologic changes. We evaluated the extravasation of fibrinogen because of intratumoral vascular leakage by immunofluorescence. Twenty-four hours following treatment, the extravasation of fibrinogen in tumor tissue was more pronounced in mice treated with CYT-6091 and CYT-21625 compared with the vehicle control and paclitaxel groups (Figure 3D). No extravasation of fibrinogen was observed in normal organs of mice treated with CYT-6091 and CYT-21625 (Figure 3E). Next, we assessed the proliferative index in the tumors treated with CYT-21625. To assess the effect of CYT-21625 on cancer cell proliferation, we evaluated proliferating cell nuclear antigen (PCNA) in xenografts as it is a nuclear protein that acts as a homotrimer and helps increase the processivity of leading strand synthesis during DNA replication. Human ATC and FTC-133 xenografts from the lungs of mice treated with CYT-21625 had statistically significantly decreased protein expression of PCNA compared with those of mice in other treatment groups (CYT-21625 vs controls, $P < .001$; CYT-21625 vs CYT-6091, $P < .001$) (Figure 3F). In addition, we observed statistically significantly increased cleaved caspase-3 protein expression in ATC and FTC-133 xenografts from the lungs of mice treated with CYT-21625 compared with other groups (CYT-21625 vs controls, $P < .001$; CYT-21625 vs CYT-6091, $P < .001$) (Figure 3G).

Tumor Selectivity of CYT-21625 in Mice With PNET

We next evaluated whether CYT-21625 selectively traffics to tumor sites using a transgenic model of PNETs. Mice 18F-FDG PET CT imaging revealed accumulation of gold nanoparticles in the PNET region 24 hours after administration of CYT-6091 and CYT-21625, which was not visualized in control mice injected with paclitaxel or vehicle control. The gold particle deposits in the area of 18F-FDG PET avidity are consistent with a selective trafficking of CYT-6091 and CYT-21625 to PNET (Figure 4).

The Effects of CYT-21625 on Tumor Vasculature in Transgenic Mouse Model of PNETs

To further evaluate whether CYT-21625 induces tumor vascular disruption and leakage in vivo, tumor vascular perfusion was measured in the transgenic PNET model using area under the curve (AUC) from DCE-MRI. The AUCs in PNETs were increased in CYT-21625- and CYT-6019-treated mice compared with mice receiving paclitaxel and vehicle control (Figure 5), consistent with the MRI contrast extravasation. The ΔAUC (between mean AUC of post-treatment and mean AUC of pretreatment) with CYT-21625 (25 187.85) and CYT-6091 (19 941.19) was increased compared with the paclitaxel (6862.80) and vehicle control (6351.82) in PNETs (Supplementary Table 1, available online). In contrast, a minimal effect was observed in muscle tissue after any treatments in all groups (Supplementary Table 1, available online). These results underscore the selective effects in the tumor tissue following administration of the targeted nanomedicine.

The Effect of CYT-21625 on Serum Insulin in Mice With Insulinomas

We evaluated the antitumor activity of CYT-21625 in *MEN1* KO mice with insulinomas by measuring the serum level of insulin, which we have previously validated as a tumor biomarker and

ARTICLE

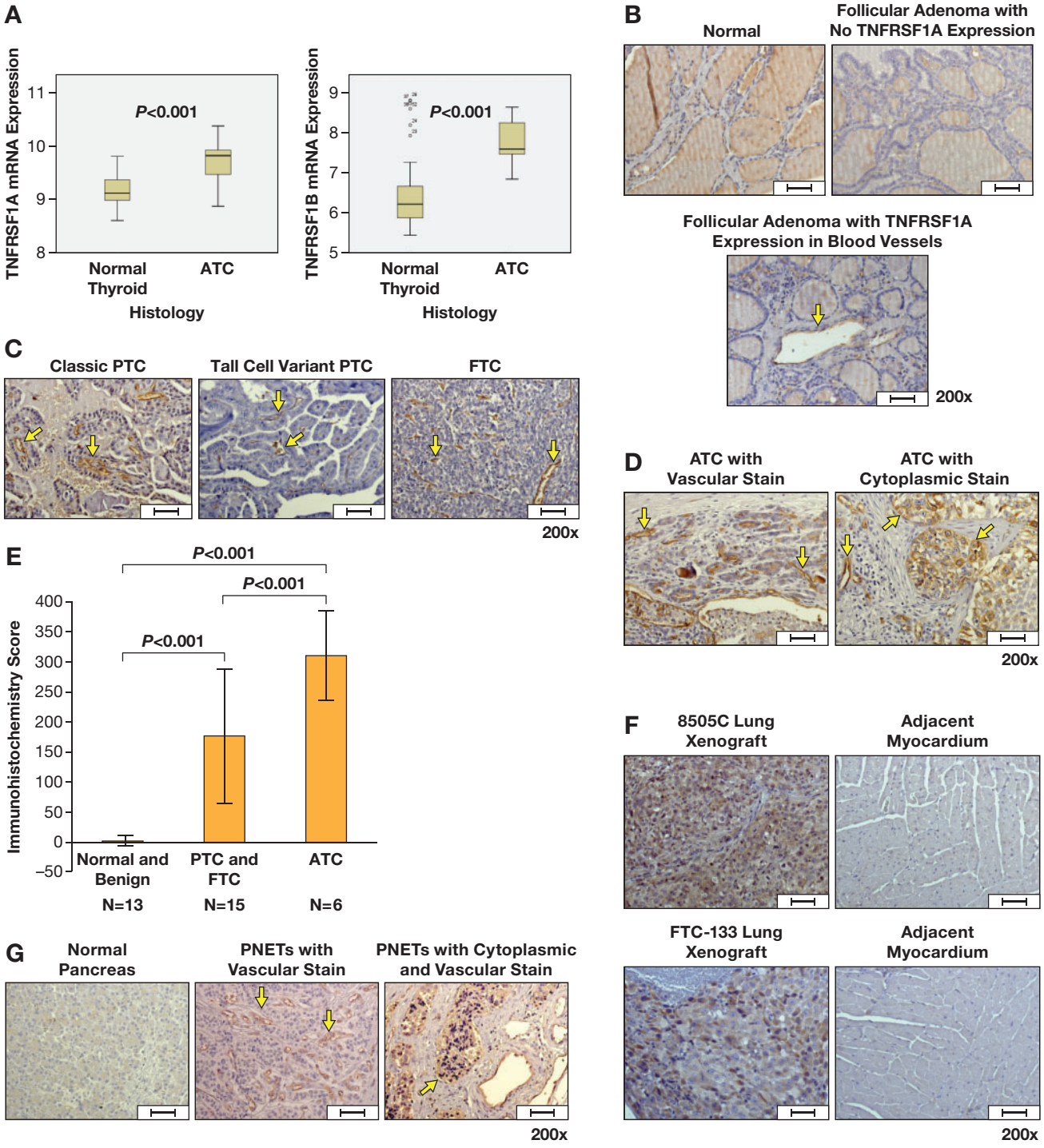

Figure 1. Tumor necrosis factor (TNF) receptor expression in normal, benign thyroid tissue, and thyroid cancers. **A)** *TNFRSF1A* and *TNFRSF1B* messenger RNA expression in anaplastic thyroid cancer (ATC) (n = 11) and normal thyroid tissue (n = 49). TNFRSF1A protein expression in **(B)** normal thyroid and follicular adenoma, **(C)** papillary thyroid cancer and follicular thyroid cancer, **(D)** ATC, **(F)** 8505C and FTC-133 lung xenografts, and **(G)** pancreatic neuroendocrine tumors and normal pancreas. Immunohistochemistry score of TNFRSF1A expression in thyroid samples is shown in **(E)**. **Arrows** indicate TNFRSF1A expression in intratumoral blood vessels. **Arrow heads (D)** indicate TNFRSF1A expression in cytoplasm. The **boxes in (A)** represent the interquartile range contaning the middle 50% of the data. The **lines across the box plot** represent the median. The **error bars** from the **upper and lower ends of the boxes** represent 1.5 times the interquatile range. **Error bars in (E)** represent standard deviation. The comparison of messenger RNA expression between groups was performed by the moderated F-statistic, which combines the t-statistics for all the pair-wise comparisons into an overall test of statistical significance for that gene. Two-side *P* values were adjusted for false discovery rate using the Benjamini and Hochberg method (27). Two-sided analysis of variance with post hoc tests was used to compare the immunohistochemistry scores. **Scale bars** = 50 μm. ATC = anaplastic thyroid cancer; FTC = follicular thyrid cancer; PNET = pancreatic neuroendocrine tumor; PTC = papillary thyroid cancer; TNFRSF1A and TNFRSF1B = tumor necrosis factor receptor superfamily, member 1A and 1B.

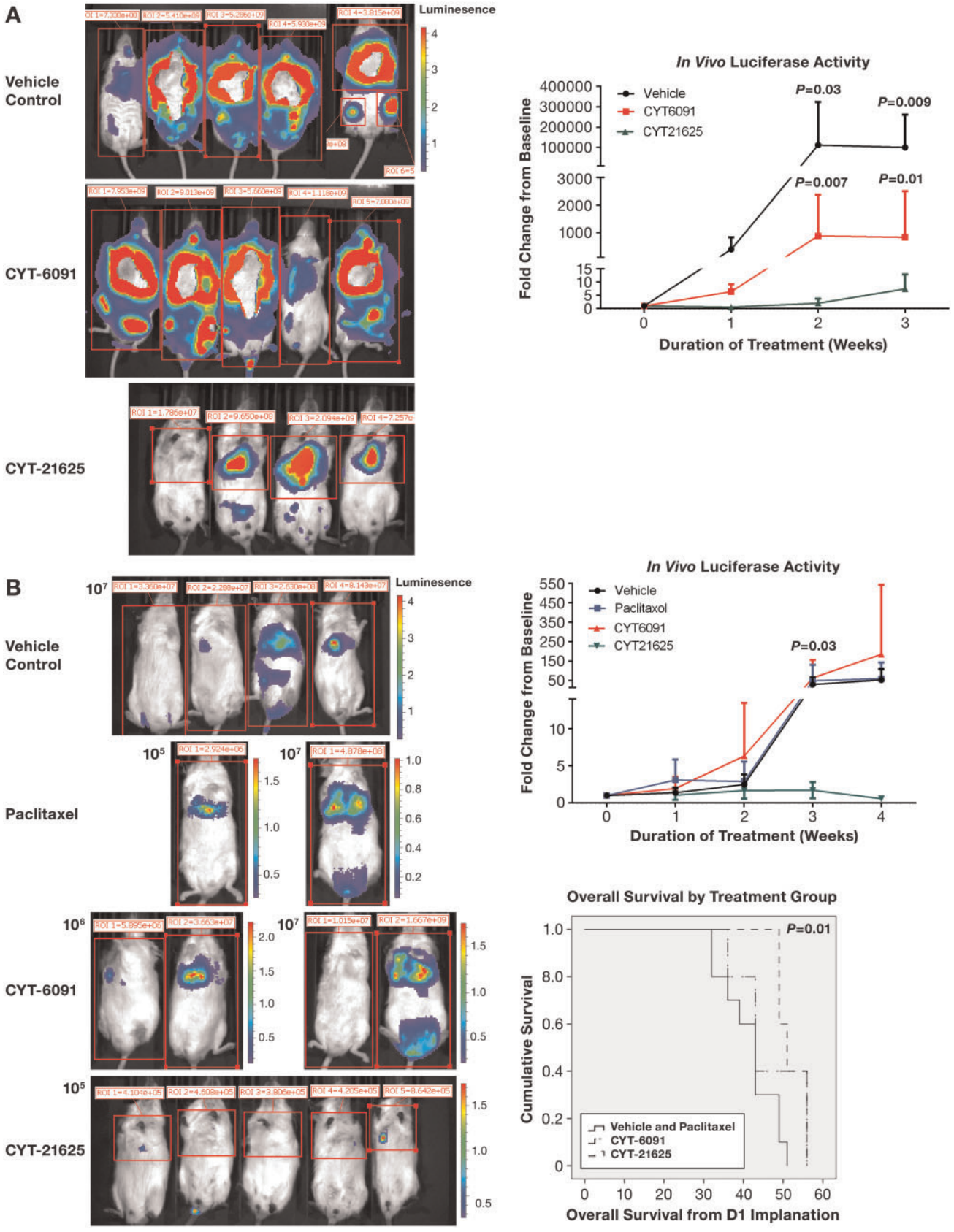

Figure 2. In vivo whole-body luciferase activity in mice. **A)** Metastatic human anaplastic thyroid cancer (8505C) xenografts. *P* values indicate statistically significant differences when the luciferase activity in mice treated with vehicle (n = 7, **black line**) and CYT-6091 (n = 6, **red line**) was compared with CYT-21625 (n = 5, **green line**). **B)** Metastatic human follicular thyroid cancer (FTC-133) xenografts. *P* values indicate statistically significant differences when the luciferase activity in mice (n = 5 per group) treated with vehicle (**black line**), paclitaxel (**blue line**), and CYT-6091 (**red line**) was compared with CYT-21625 (**green line**). The two-sided Student *t* test was used to assess the difference in luciferase activity between groups.

ARTICLE

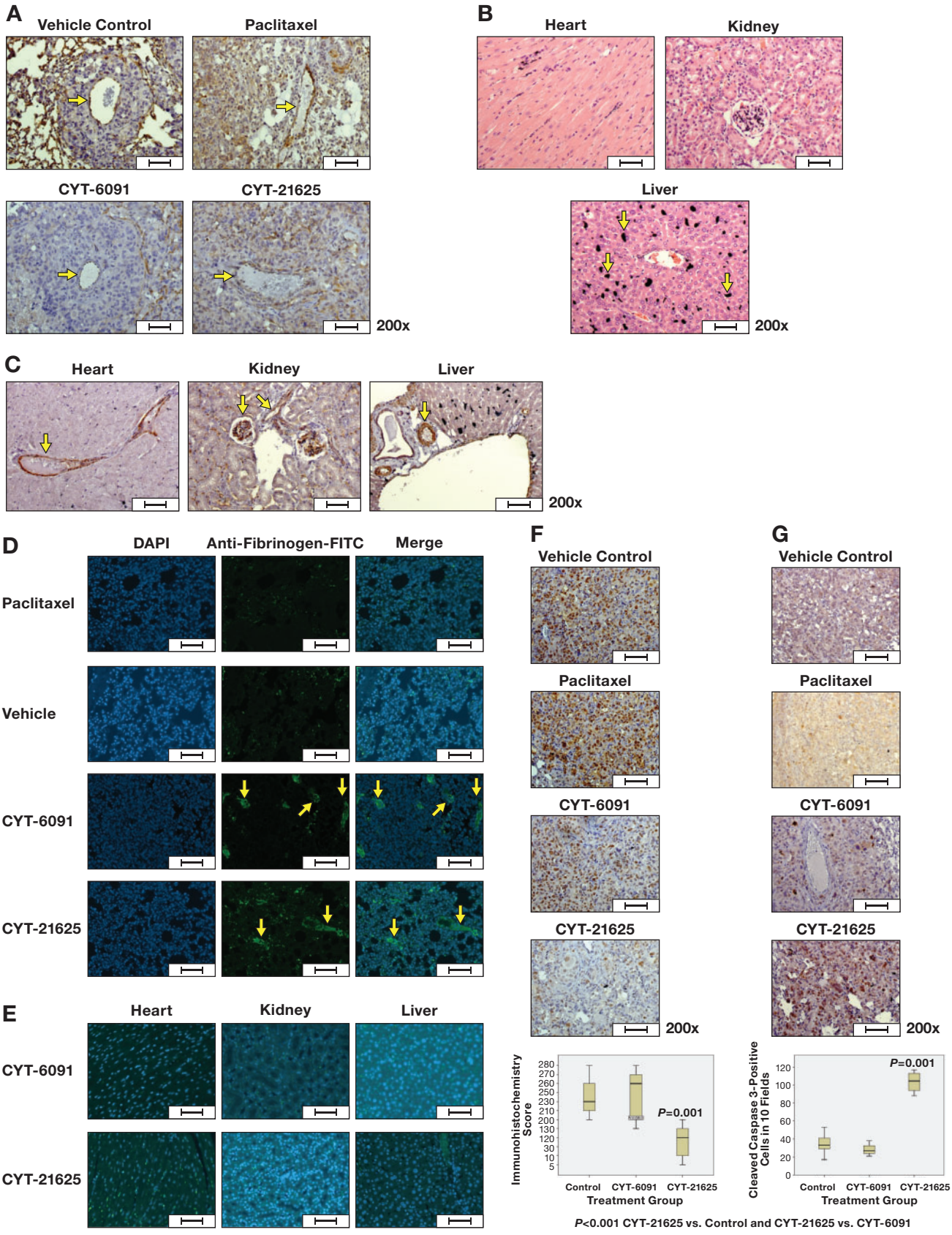

Figure 3. Hematoxylin and eosin (H&E), immunohistochemistry, and immunofluorescence staining of metastatic anaplastic thyroid cancer (8505C) xenograft and normal organs (heart, liver, and kidney) in mice treated with CYT-21625, CYT-6091, paclitaxel, and vehicle. **A)** CD34 expression in intratumoral blood vessels (**arrows**), **(B)** H&E staining of normal organs (**arrows** indicate gold nanoparticles deposit), **(C)** CD34 expression in vascular endothelium of normal organs (**arrows**), **(D)** the extravasation of fibrinogen in 8505C xenografts (**arrows**) and in **(E)** normal organs of mice treated with CYT-6091 and CYT-21625 (Merge (DAPI+Anti-fibrinogen)), **(F)** proliferating cell nuclear antigen in 8505C and FTC-133 xenografts, and **(G)** cleaved caspase-3 expression in 8505C and FTC-133 xenografts. The **boxes in (A)** represent the interquartile range contaning the middle 50% of the data. The **lines across the box plot** represent the median. The **error bars** from the **upper and lower ends of the boxes** represent 1.5 times the interquatile range. Two-sided analysis of variance with post hoc tests was used to compare the immunohistochemistry scores. **Scale bars** = 50 μm.

ARTICLE

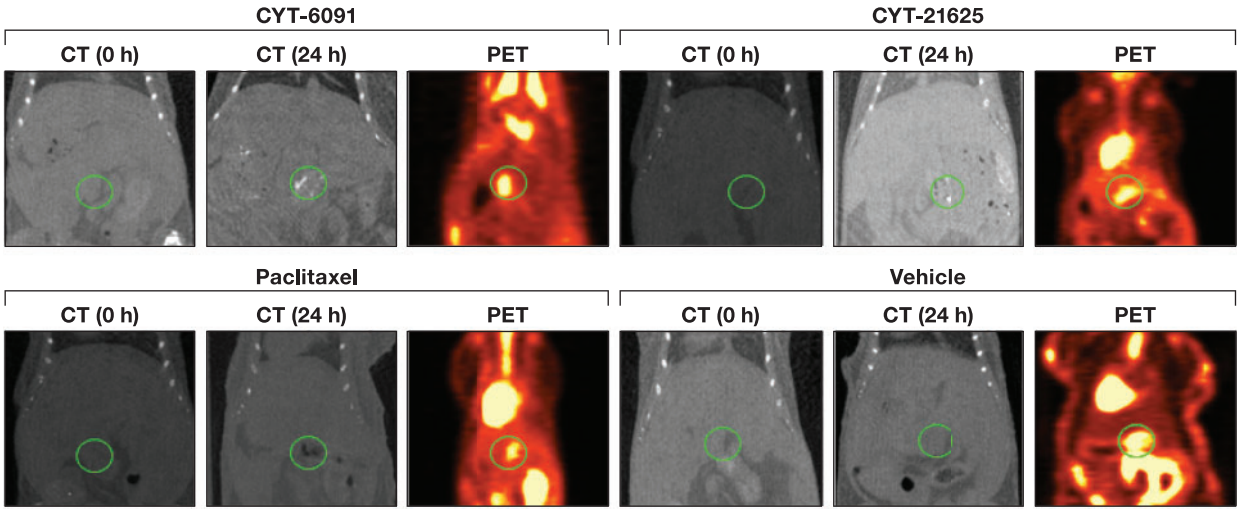

Figure 4. In vivo evaluation of biodistribution of CYT-21625 by computed tomography (CT) and 18F-FDG positron emission tomography (PET) scan. CT shows increased gold particle density in the pancreatic region (**circle**) in the multiple endocrine neoplasia type 1 gene knock-out mice treated with CYT-6091 and CYT-21625 at 24 hours postinjection (**top**), but not in the mice treated with paclitaxel and vehicle control (**bottom**). 18F-FDG PET images demonstrate pancreatic neuroendocrine tumor location in the midabdominal area, corresponding with the area where gold particles deposited. CT = computed tomography; PET = positron emission tomography.

surrogate for tumor response to therapy (26,32). Baseline serum insulin levels in all four groups (CYT-21625, CYT-6091, paclitaxel, and vehicle control) were measured, with no statistically significant difference: 3.617 μg/L ± 0.061, 3.580 μg/L ± 0.160, 3.580 μg/L ± 0.105, and 3.543 μg/L ± 0.078, respectively ($P = .87$). By day 7 after administration, mice treated with CYT-21625 had statistically significant lower serum insulin levels (1.927 ± 0.231 μg/L) than those treated with CYT-6091 (3.010 ± 0.130 μg/L, $P = .001$), paclitaxel (2.943 ± 0.239 μg/L, $P = .001$), and vehicle control (3.693 ± 0.035 μg/L, $P < .001$). Furthermore, we observed that mice receiving CYT-21625 had the largest decrease in their serum insulin levels when compared with those receiving treatment with either CYT-6091 or paclitaxel at seven and 14 days post-treatment ($P < .001$) (Figure 6). After 28 days of treatment, all three mice treated with CYT-21625 survived, and their insulin levels continued to decrease to 0.59 μg/L ± 0.151. Two mice in CYT-6091 and one each in the paclitaxel- and vehicle-treated groups survived on day 28. However, the insulin levels in mice treated with vehicle control, paclitaxel, and CYT-6091 were all higher than 3 μg/L.

Discussion

CYT-21625 is the first-in-class nanomedicine that specifically addresses the high tumor IFP that limits efficacy of current systemic therapy by targeting and disrupting tumor vasculature and delivers paclitaxel to cancer cells. We evaluated the efficacy of a novel nanomedicine, CYT-21625, in a transgenic and metastatic mouse model of endocrine cancers. Because CYT-21625 selectively targets intratumoral blood vessels passively by EPR effect and actively by rhTNF, we first demonstrated, using gene expression profiling analysis and tissue microarray, that all human ATC samples and half of differentiated thyroid cancer samples overexpressed TNFRSF1A mRNA and protein in blood vessels and/or tumor cell cytoplasm. Because the normal thyroid tissue samples in GSE33630 were from patients with post-Chernobyl PTC, commonly associated with lymphocytic thyroiditis, high expression of TNFRSF1B mRNA can be from regulatory T cells found in lymphocytic thyroiditis (33). In addition, eight of 13 primary PNET samples expressed TNFRSF1A in intratumoral blood vessels, including one in cytoplasm. The results suggest that CYT-21625 can preferentially target differentiated thyroid cancers, ATC, and PNETs. CYT-21625 was effective in mice with metastatic human ATC cells, as demonstrated by a statistically significantly lower tumor burden in the CYT-21625-treated group. We observed a statistically significantly lower tumor burden in mice with metastatic human FTC in the CYT-21625 group after three weeks of treatment. Although the difference in luciferase activity did not reach statistical significance in mice with metastatic FTC-133 xenografts on week 4 because of type II error from reduced sample size as three mice in the non-CYT-21625 group died after week 3 treatment, the average luciferase activity on week 4 was even lower than the baseline, suggesting the efficacy of CYT-21625 in reducing tumor burden. A larger sample size would provide sufficient power to show the difference. Immunohistochemistry showed decreased cell proliferation, increased apoptosis, loss of CD34 expression in tumor vasculature, and vascular leakage demonstrated by extravasation of fibrinogen, consistent with the effect of rhTNF. Animals tolerated CYT-21625 with no histologic evidence of normal organ toxicity. Furthermore, we used DCE-MRI to demonstrate the enhanced vascular permeability in *MEN1* KO mice with PNETs treated with CYT-6091 and CYT-21625. CT and PET scans showed a selective accumulation of CYT-6091 and CYT-21625 in the PNETs of the mice. A statistically significant, progressive, and time-dependent decrease in serum insulin level was observed in *MEN1* KO mice with insulinomas treated with CYT-21625 (26). The results warrant a clinical study to determine the efficacy of CYT-21625 as a novel therapy for advanced PDTC, ATC, and PNET.

CYT-21625 maximizes efficacy and minimizes off-target effects by targeting tumor vasculature and delivering paclitaxel analogue to tumor cells. We demonstrated that CYT-6091, a precursor of CYT-21625, comprised of rhTNF bound to 27 nm PEGylated gold nanoparticles without paclitaxel analogue, caused tumor vascular disruption and statistically significantly reduced IFP in vivo (34). A phase I clinical trial showed that CYT-6091 was well tolerated, and dose-limiting toxicity did not occur at a dosage exceeding three times the systemically administered native rhTNF (35). Colloid gold is a nanoparticle that

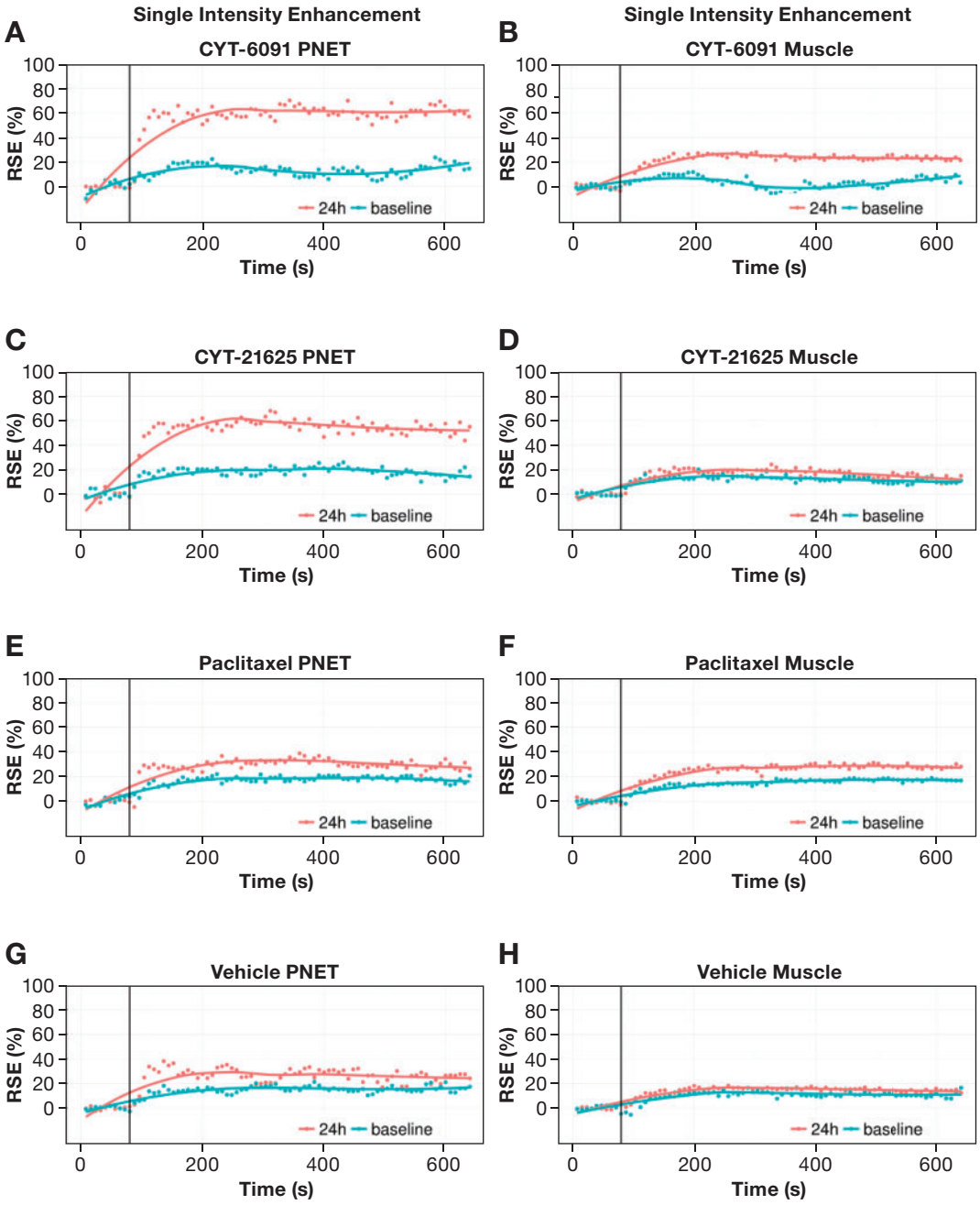

Figure 5. Imaging vascular effects of CYT-21625 by dynamic contrast-enhanced magnetic resonance imaging (DCE-MRI). The signal enhancement curve was used for quantifying the tumor vasculature **(A, C, E, G)** and control muscle vasculature **(B, D, F, H)** by DCE-MRI. The first six time points are pre–injection of gadolinium with diethylenetriaminepentacetate (Gd-DTPA); the next 80 are post–injection of Gd-DTPA. E(t) = [S(Ct)-S(0)]/S(0), where S(0) is the signal absence of Gd-DTPA (Ct = 0) and S(Ct) is the signal after injection of Gd-DTPA. The data are from the pancreatic and control muscle regions of multiple endocrine neoplasia type 1 gene knock-out mice (n = 3) at 24 hours postinjection **(red curve)** and baseline **(green curve)**. PNET = pancreatic neuroendocrine tumor; RSE = Relative signal enhancement.

is a good delivering system for proteins such as rhTNF because it strongly and preferentially binds to these molecules through the available thiol group (20). Colloidal gold has been safely used clinically for decades in the treatment of rheumatoid arthritis, and radio-gold colloids have been used in various human therapeutics (36,37). This suggests that colloidal gold particles should be a safe platform for a new drug delivery system. However, the antitumor effect of rhTNF alone is minimal, while the combination of rhTNF followed by chemotherapy can result in a dramatic response (38,39). It has been proposed that rhTNF induces vascular hyperpermeability in the tumor, which enhances the efficacy of chemotherapy. The clinical evidence supporting this concept is best exemplified by the results of isolated hyperthermic limb perfusion with rhTNF and melphalan for in-transit melanoma or sarcoma, where overall response rates ranged from 75% to 100% (40–42). In this study, we show a superior antitumor effect of CYT-21625 that combined the results of intratumoral vascular disruption from rhTNF and the antiproliferation effect from paclitaxel. Compared with mice treated with intravenous paclitaxel, treatment with CYT-21625

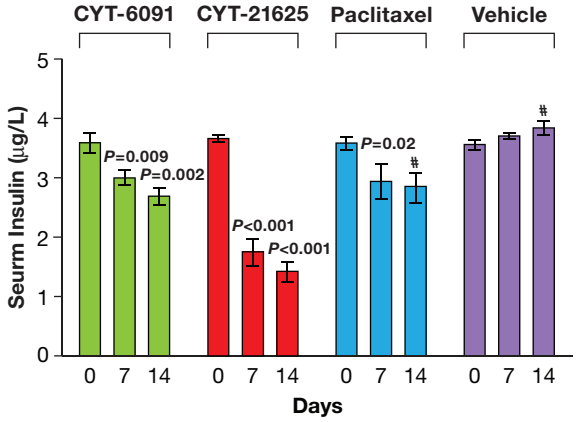

Figure 6. Antitumor activity of CYT-21625 was evaluated in *MEN1* KO mice. Serum insulin levels were measured using an enzyme-linked immunosorbent assay at baseline and 7 and 14 days after treatment with CYT-6091, CYT-21625, paclitaxel, or vehicle (n = 3 per group). One mouse each in the paclitaxel-treated and vehicle control (phosphate-buffered saline–treated) groups died. The statistical significance within each of the four groups was calculated compared with their respective baselines using a two-sided Student *t* test. **Error bars** represent standard deviation. At day 14, one mouse died in the paclitaxel group and one died in the vehicle control group.

delivering the same dose of paclitaxel resulted in statistically significant lower tumor burden, suggesting a more effective delivery system. Because CYT-21625 actively targets TNFRSF1A and passively targets tumor vasculature by enhanced permeability and retention effect, we believe CYT-21625 should still be effective in tumors with low TNFRSF1A expression at the appropriate dosage. Further study in TNFRSF1A-negative tumors is warranted. Although we observed CYT-6091 and CYT-21625 in the liver, there were no other histologic changes in hepatocytes or vascular leakage that suggest liver toxicity. The liver deposition may be from the mononuclear phagocyte system scavenging the gold nanoparticles. The increased AUC in DCE-MRI is consistent with the effect of rhTNF in CYT-6091 and CYT-21625 that caused vascular hyperpermeability and the detection of MRI contrast in tumor tissue (43). The histologic confirmation of vascular leakage was demonstrated by the extravasation of fibrinogen in the tumor tissue of mice treated with nanomedicines. The extravasation and deposition of clotting factors such as fibrinogen is used to demonstrate an increased vascular permeability (44). CYT-21625 preferentially and selectively targeted tumors as demonstrated by CT, PET, and MRI without evidence of off-target effects on histologic examination of normal organs.

There have been few studies in thyroid cancers that investigate the antitumor efficacy of nanoparticles carrying various payloads such as chemotherapeutics, radioisotopes, and small interfering RNA (siRNA) to silence oncogenes (45–47). Paolino et al. demonstrated the improved in vitro and in vivo efficacy of thyroid-stimulating hormone (TSH) conjugated nanoliposomes encapsulated with gemcitabine in FTC-133 cells (47). However, PDTC and ATC often have low or absent expression of the TSH receptor, which could affect the efficacy of this delivery system. In this study, we show that CYT-21625 was effective in PDTC, ATC, and PNETs. It is possible that CYT-21625 could be effective in a wide range of solid cancers, as it specifically targets tumor vasculature and then delivers the paclitaxel to the tumor. In contrast to other systems delivering siRNA (46) or a novel radioisotope (45) without any known safety profiles, CYT-21625 delivers rhTNF and paclitaxel, which have been used clinically with known toxicity profiles. Unlike an siRNA delivery system, CYT-21625 does not require specific mutations and can be effective in a broad range of solid cancers. Because pharmacokinetics and toxicity profiles of paclitaxel and CYT-6091, a prototype of CYT-21625 without paclitaxel, have been well studied in clinical trials (35), we anticipate that the CYT-21625 will be well tolerated in patients with advanced thyroid cancers, PNETs, and other solid tumors. Pazopanib, a multikinase inhibitor affecting tumor vasculature, potentiates the antitumor effects of paclitaxel in vitro and in vivo (48). Currently, a randomized, phase II clinical trial that studies the effects of intensity-modulated radiotherapy and paclitaxel with and without pazopanib is ongoing. CYT-21625 uses a similar concept to target and disrupt tumor vasculature, specifically delivers paclitaxel, to tumor cells. Thus, fewer off-target adverse effects are expected than with systemically administered treatments.

CYT-21625 requires tissue GSH to release paclitaxel analogue to the cells; thus, in vitro studies of cells treated with CYT-21625 are not feasible. However, the mechanisms of action of paclitaxel are well studied (49). Although the maximum tolerated dose of CYT-21625 in mice is not yet known, we anticipated it to be several times higher than the equivalent doses of intravenous rhTNF and paclitaxel, as demonstrated in a phase I clinical trial of CYT-6091 (35). It is possible that CYT-21625 may be more effective at a higher dose. In addition, the flexibility of the gold nanoparticles system in delivering various payloads may be further explored. Gold nanoparticles have been used in diagnostic and photothermal and photodynamic therapy (50). CYT-6091 combined with radiation reduced tumor IFS and resulted in synergistic antitumor response in vivo (34).

The limitations of this study included small sample size in mice with FTC-133 xenografts. Although the tumor burden in mice treated with CYT-21625 was lower than other groups after four weeks of treatments, the difference did not reach statistical significance due to type II error, as mice in the non-CYT-21625 group died. In addition, the lack of definitive marker specifically for cellular effect caused by paclitaxel makes the assessment of the antiproliferative mechanism difficult. We are unable to specify whether the antitumor effect was caused by rhTNF or paclitaxel or both.

In summary, we demonstrated that PDTC, ATC, and PNETs are suitable targets for CYT-21625. CYT-21625 treatment in mice with metastatic human PDTC and ATC resulted in a smaller tumor burden by inducing tumor vascular endothelial damage, vascular leakage, and apoptosis, and by decreasing cell proliferation without toxicity. Tumor selectivity and the increased tumor vascular permeability were demonstrated by CT, PET, and DCE-MRI in *MEN1* KO mice with insulinomas and by histology in mice with metastatic human PDTC and ATC xenografts. CYT-21625 effectively reduced serum insulin in mice with insulinomas. Thus, CYT-21625 is a promising novel therapy that should be studied in patients with advanced PDTC, ATC, and PNETs.

Funding

This work was supported by the intramural research program of the Center for Cancer Research, National Cancer Institute (ZIA BC01128607), and was supported in part by SBIR grant R43 CA119399 from the National Cancer Institute and a grant from the Maryland Technology Development Corporation (TEDCO; "Development and Pilot Manufacturing for Multi-functional Tumor Targeting Nanomedicine").

ARTICLE

Notes

Affiliations of authors: Endocrine Oncology Branch, National Cancer Institute, National Institutes of Health, Bethesda, MD (NN, KG, EMF, EK); Department of Surgery, Albert Einstein College of Medicine, Bronx, NY (ZY, CS, SKL); CytImmune Sciences, Inc., Rockville, MD (GFP, LT); Department of Chemistry and the Virginia Tech Center for Drug Discovery, Blacksburg, VA (SC, JZ, DGIK).

The funders had no role in the design of the study; the collection, analysis, or interpretation of the data; the writing of the manuscript; or the decision to submit the manuscript for publication.

The authors declare no conflict of interest.

Study design: NN, ZY, GP, LT, SL, EK; conducting experiments: NN, ZY, GP, CS, KG, EF, SC, JZ, DK; acquiring and analyzing data: NN, ZY, GP, LT, SL, EK; manuscript preparation: NN, ZY, GP, LT, CS, KG, EF, SC, JZ, DK, SL, EK.

References

1. Brose MS, Nutting CM, Jarzab B, et al. Sorafenib in radioactive iodine-refractory, locally advanced or metastatic differentiated thyroid cancer: A randomised, double-blind, phase 3 trial. *Lancet*. 2014;384(9940):319–328.
2. Schlumberger M, Tahara M, Wirth LJ, et al. Lenvatinib versus placebo in radioiodine-refractory thyroid cancer. *N Engl J Med*. 2015;372(7):621–630.
3. Davies L, Welch HG. Increasing incidence of thyroid cancer in the United States, 1973-2002. *JAMA*. 2006;295(18):2164–2167.
4. Kebebew E, Greenspan FS, Clark OH, et al. Anaplastic thyroid carcinoma. *Treatment outcome and prognostic factors*. *Cancer*. 2005;103(7):1330–1335.
5. Smallridge RC, Ain KB, Asa SL, et al. American Thyroid Association guidelines for management of patients with anaplastic thyroid cancer. *Thyroid*. 2012; 22(11):1104–1139.
6. Kebebew E. Anaplastic thyroid cancer: Rare, fatal, and neglected. *Surgery*. 2012;152(6):1088–1089.
7. Halfdanarson TR, Rubin J, Farnell MB, et al. Pancreatic endocrine neoplasms: Epidemiology and prognosis of pancreatic endocrine tumors. *Endocr Relat Cancer*. 2008;15(2):409–427.
8. Krampitz GW, Norton JA. Pancreatic neuroendocrine tumors. *Curr Probl Surg*. 2013;50(11):509–545.
9. Oberg K. Pancreatic endocrine tumors. *Semin Oncol*. 2010;37(6):594–618.
10. Bilimoria KY, Tomlinson JS, Merkow RP, et al. Clinicopathologic features and treatment trends of pancreatic neuroendocrine tumors: Analysis of 9,821 patients. *J Gastrointest Surg*. 2007;11(11):1460–1467; discussion 1467–1469.
11. Franko J, Feng W, Yip L, et al. Non-functional neuroendocrine carcinoma of the pancreas: Incidence, tumor biology, and outcomes in 2,158 patients. *J Gastrointest Surg*. 2010;14(3):541–548.
12. Hill JS, McPhee JT, McDade TP, et al. Pancreatic neuroendocrine tumors: The impact of surgical resection on survival. *Cancer*. 2009;115(4):741–751.
13. Yao JC, Shah MH, Ito T, et al. Everolimus for advanced pancreatic neuroendocrine tumors. *N Engl J Med*. 2011;364(6):514–523.
14. Raymond E, Dahan L, Raoul JL, et al. Sunitinib malate for the treatment of pancreatic neuroendocrine tumors. *N Engl J Med*. 2011;364(6):501–513.
15. Heldin CH, Rubin K, Pietras K, et al. High interstitial fluid pressure - an obstacle in cancer therapy. *Nat Rev Cancer*. 2004;4(10):806–813.
16. Papini E, Guglielmi R, Bianchini A, et al. Risk of malignancy in nonpalpable thyroid nodules: Predictive value of ultrasound and color-Doppler features. *J Clin Endocrinol Metab*. 2002;87(5):1941–1946.
17. Utsumi M, Umeda Y, Takagi K, et al. Correlation of computed tomography imaging features and pathological features of 41 patients with pancreatic neuroendocrine tumors. *Hepatogastroenterology*. 2015;62(138):441–446.
18. Gabizon A, Bradbury M, Prabhakar U, et al. Cancer nanomedicines: Closing the translational gap. *Lancet*. 2014;384(9961):2175–2176.
19. Gamcsik MP, Kasibhatla MS, Teeter SD, et al. Glutathione levels in human tumors. *Biomarkers*. 2012;17(8):671–691.
20. Paciotti GF, Myer L, Weinreich D, et al. Colloidal gold: A novel nanoparticle vector for tumor directed drug delivery. *Drug Deliv*. 2004;11(3):169–183.
21. van Staveren WC, Solis DW, Delys L, et al. Human thyroid tumor cell lines derived from different tumor types present a common dedifferentiated phenotype. *Cancer Res*. 2007;67(17):8113–8120.
22. Zhang L, Gaskins K, Yu Z, et al. An in vivo mouse model of metastatic human thyroid cancer. *Thyroid*. 2014;24(4):695–704.
23. Edgar R, Domrachev M, Lash AE. Gene Expression Omnibus: NCBI gene expression and hybridization array data repository. *Nucleic Acids Res*. 2002;30(1): 207–210.
24. Tomas G, Tarabichi M, Gacquer D, et al. A general method to derive robust organ-specific gene expression-based differentiation indices: Application to thyroid cancer diagnostic. *Oncogene*. 2012;31(41):4490–4498.
25. Jiao Y, Shi C, Edil BH, et al. DAXX/ATRX, MEN1, and mTOR pathway genes are frequently altered in pancreatic neuroendocrine tumors. *Science*. 2011; 331(6021):1199–1203.
26. Shen HC, He M, Powell A, et al. Recapitulation of pancreatic neuroendocrine tumors in human multiple endocrine neoplasia type I syndrome via Pdx1-directed inactivation of Men1. *Cancer Res*. 2009;69(5):1858–1866.
27. Benjamini Y, Hochberg Y. Controlling the false discovery rate - a practical and powerful approach to multiple testing. *J Royal Stat Soc Ser B Methodol*. 1995;57(1):289–300.
28. Student. The probable error of a mean. *Biometrika*. 1908;6(1):1–25.
29. Kaplan EL, Meier P. Nonparametric estimation from incomplete observations. *J Am Stat Assoc*. 1958;53:457–481.
30. Mantel N. Evaluation of survival data and two new rank order statistics arising in its consideration. *Cancer Chemother Rep*. 1966;50(3):163–170.
31. R Development Core Team. *R: A Language and Environment for Statistical Computing*. Vienna, Austria: R Foundation for Statistical Computing; 2010. http://www.R-project.org.
32. Quinn TJ, Yuan Z, Adem A, et al. Pasireotide (SOM230) is effective for the treatment of pancreatic neuroendocrine tumors (PNETs) in a multiple endocrine neoplasia type 1 (MEN1) conditional knockout mouse model. *Surgery*. 2012;152(6):1068–1077.
33. Ellis JS, Hong SH, Zaghouani H, et al. Reduced effectiveness of CD4+Foxp3+ regulatory T cells in CD28-deficient NOD.H-2h4 mice leads to increased severity of spontaneous autoimmune thyroiditis. *J Immunol*. 2013;191(10): 4940–4949.
34. Koonce NA, Quick CM, Hardee ME, et al. Combination of gold nanoparticle-conjugated tumor necrosis factor-alpha and radiation therapy results in a synergistic antitumor response in murine carcinoma models. *Int J Radiat Oncol Biol Phys*. 2015;93(3):588–596.
35. Libutti SK, Paciotti GF, Byrnes AA, et al. Phase I and pharmacokinetic studies of CYT-6091, a novel PEGylated colloidal gold-rhTNF nanomedicine. *Clin Cancer Res*. 2010;16(24):6139–6149.
36. Graham-Bonnalie FE. Gold for rheumatoid arthritis. *Br Med J*. 1971;2(5756): 277.
37. Root SW, Andrews GA, Kniseley RM, et al. The distribution and radiation effects of intravenously administered colloidal Au198 in man. *Cancer*. 1954; 7(5):856–866.
38. van Horssen R, Ten Hagen TL, Eggermont AM. TNF-alpha in cancer treatment: Molecular insights, antitumor effects, and clinical utility. *Oncologist*. 2006;11(4):397–408.
39. ten Hagen TL, Eggermont AM. Solid tumor therapy: Manipulation of the vasculature with TNF. *Technol Cancer Res Treat*. 2003;2(3):195–203.
40. Alexander HR Jr, Fraker DL, Bartlett DL. Isolated limb perfusion for malignant melanoma. *Semin Surg Oncol*. 1996;12(6):416–428.
41. Fraker DL, Alexander HR, Andrich M, et al. Treatment of patients with melanoma of the extremity using hyperthermic isolated limb perfusion with melphalan, tumor necrosis factor, and interferon gamma: Results of a tumor necrosis factor dose-escalation study. *J Clin Oncol*. 1996;14(2): 479–489.
42. Eggermont AM, Schraffordt Koops H, Klausner JM, et al. Isolated limb perfusion with tumor necrosis factor and melphalan for limb salvage in 186 patients with locally advanced soft tissue extremity sarcomas. The cumulative multicenter European experience. *Ann Surg*. 1996;224(6):756–764; discussion 764–765.
43. Skinner JT, Moots PL, Ayers GD, et al. On the use of DSC-MRI for measuring vascular permeability. *Am J Neuroradiol*. 2016;37(1):80–87.
44. Muradashvili N, Benton RL, Saatman KE, et al. Ablation of matrix metalloproteinase-9 gene decreases cerebrovascular permeability and fibrinogen deposition post traumatic brain injury in mice. *Metab Brain Dis*. 2015; 30(2):411–426.
45. Zhou M, Chen Y, Adachi M, et al. Single agent nanoparticle for radiotherapy and radio-photothermal therapy in anaplastic thyroid cancer. *Biomaterials*. 2015;57:41–49.
46. Ali HM, Maksimenko A, Urbinati G, et al. Effects of silencing the RET/PTC1 oncogene in papillary thyroid carcinoma by siRNA-squalene nanoparticles with and without fusogenic companion GALA-cholesterol. *Thyroid*. 2014;24(2): 327–338.
47. Paolino D, Cosco D, Gaspari M, et al. Targeting the thyroid gland with thyroid-stimulating hormone (TSH)-nanoliposomes. *Biomaterials*. 2014; 35(25):7101–7109.
48. Isham CR, Bossou AR, Negron V, et al. Pazopanib enhances paclitaxel-induced mitotic catastrophe in anaplastic thyroid cancer. *Sci Transl Med*. 2013;5(166):166ra3.
49. Horwitz SB. Taxol (paclitaxel): Mechanisms of action. *Ann Oncol*. 1994;5(suppl 6):S3–S6.
50. Guo J, Rahme K, He Y, et al. Gold nanoparticles enlighten the future of cancer theranostics. *Int J Nanomed*. 2017;12:6131–6152.